Photoelectrolysis of glucose and fructose containing solution in PGM-free cells for hydrogen and valuable chemicals production

Claudio M. Pecoraro, Francesco Di Franco, Vittorio Loddo, Marianna Bellardita, Monica Santamaria*

Dipartimento di Ingegneria, Università degli Studi di Palermo, Viale delle Scienze Edificio 6, 90128 Palermo, Italy

*monica.santamaria@unipa.it

Abstract

This study investigates the anaerobic partial oxidation of glucose and fructose using photoelectrocatalysis, employing TiO_2 NTs photoanodes and Ni foam as the cathode for the Hydrogen Evolution Reaction. TiO_2 NTs were grown on Ti felt via anodization and annealed to promote crystallization, resulting in photoanodes with both high stability and photoactivity that can be reused after a proper cleaning step.

These electrodes were tested in an aqueous solution with a pH range from 2 to 12, both with and without the addition of biomass. When biomass was present, the hydrogen production rate increased, reaching faradic efficiencies (FEs) ~ 100%, allowing the simultaneous production of valuable partial oxidation compounds, such as gluconic acid (GA) and formic acid (FA).

The results demonstrated that this photoelectrocatalytic (PEC) process is promising for biomass oxidation and H_2 production, highlighting the advantages of PEC systems in achieving efficient and selective biomass conversion.

Keywords
Biomass partial oxidation, H_2 production, Photoelectrocatalysis, TiO_2 nanotubes, Pt-free electrodes

Highlights

- Photoelectroreforming of glucose and fructose to produce H_2, GA, and FA was studied
- TiO_2 NTs on Ti felt and Pt-free Ni foam were utilized as the photoanode and cathode, respectively

- A H_2 faradaic efficiency of 100% was achieved
- Both electrodes showed high mechanical and chemical stability, allowing reusability

1. Introduction

The depletion of fossil fuel reserves and the increasing environmental pollution have encouraged the scientific community's interest in renewable energy sources and, among them, H_2 stands out as a promising clean energy carrier [1–4]. In this context, a promising approach as an ideal and sustainable alternative to fossil resource utilization involves converting renewable biomass into H_2 and valuable chemicals [5–7].

Glucose and its isomer fructose, derived directly from cellulose, are the most abundant and renewable biomasses on Earth [8]. They can serve as precursors for producing ethanol, renewable diesel, and jet fuels, along with a wide array of biobased chemicals used as industrial feedstocks for bioplastics and hydrogen production [9–13]. Notably, the selective oxidation of these compounds to produce gluconic and formic acids is particularly appealing due to their industrial applications as platform chemicals.

Gluconic acid (GA) and its derivatives market values are expected to reach \$1.9 billion by 2028 and find extensive use in the food, pharmaceutical, and detergent industries as flavoring and chelating agents [14,15]. Moreover, formic acid (FA) serves as an energy carrier and is a crucial intermediate in chemical synthesis across industries ranging from chemical and agricultural to pharmaceutical, textile, and rubber. Its market value is expected to increase up to \$4 billion in the next 10 years [16,17].

Various technologies involving high temperature and pressure conditions have been employed to obtain GA and FA, obtaining low selectivity, difficult separation, pollutant emissions, and low yields, despite the use of expensive catalysts, oxidizing agents, harsh reaction conditions, and high energy consumption [18–20]. Therefore, there's a high demand for alternative methods for glucose and fructose conversion.

Photoelectrocatalysis (PEC) in aqueous solutions at ambient conditions emerges as a promising, environmentally friendly, and efficient alternative to chemical and enzymatic methods. PEC can be employed in biomass oxidation, H_2 production, and organic synthesis, combining renewable feedstock and green energy sources to concurrently produce building-block chemicals and clean fuel [21–26].

Within PEC systems, photoinduced electrons (e^-) and holes (h^+) can migrate through the applied electric field, with electrons moving to the cathode and holes to the surfaces of the photoanode. This charge redistribution results in reduction and oxidation reactions occurring at these respective electrodes [27–29]. Despite extensive research on PEC systems for water splitting [30–32] and organic pollutant degradation [33–35], investigations into PEC oxidation of organic compounds remain relatively limited. Notably, the main challenge in PEC oxidation of organic compounds lies in achieving high selectivity towards desired products and high faradic efficiency (FE) [25]. As a photoanode, TiO_2 stands out as the leading choice in PEC systems due to its exceptional photocatalytic activity, high stability, scalability, cost-effectiveness, and non-toxic properties [36–40]. This study focuses on the anaerobic partial oxidation of glucose and fructose in an aqueous medium under mild temperature and pressure conditions to produce H_2 and high-value-added (HVA) products. As the electrodes, platinum group metal (PGM) free TiO_2 nanotubes (NTs) as the photoanode and Ni foam as the cathode were used. Notably both the electrodes showed a high chemical and physical stability since they were used for each test after a proper cleaning step. The influence of TiO_2 NTs features and pH of the reaction medium on HVA products and H_2 FEs were studied for both glucose and fructose.

2. Experimental

2.1. Electrodes preparation

TiO_2 nanotube photoanodes were fabricated by anodization [25,40,41]. Titanium fiber felt (Fuel cell store) with a thickness ranging from 0.2 to 0.3 mm was cut and etched for 2 seconds in a solution containing hydrofluoric acid (Sigma Aldrich, purity 39.5%), nitric acid (Sigma Aldrich, purity 69.0%), and deionized water at a volume ratio of 1:1:3. Subsequently, they were sonicated in acetone and ethanol for 5 minutes each, followed by rinsing with deionized water and air-drying. Anodization was carried out in a two-electrode cell setup, with aluminum foil serving as the cathode in an ethylene glycol solution (EG, Aldrich, 99.8% anhydrous) containing NH_4F (Sigma Aldrich) and deionized water. TiO_2 nanotubes with different features were obtained by varying the anodization conditions, i.e., the composition of the anodization bath, time, and potential. The synthesis conditions are reported in Table 1.

Table 1. Composition of anodization bath, potential, and time of the two samples

Sample	EG (%wt)	NH_4F (%wt)	H_2O (%wt)	Potential (V)	Time (min)
0.75%w	99	0.25	0.75	45	10
50%w	49.5	0.5	50	30	30

Soon after the anodization step, both samples were annealed in air to 450°C for 3 hours to promote the crystallization of the TiO_2 nanotubes towards the anatase phase.
Commercial Ni foam (Goodfellow) was employed as the cathode.

2.2. Characterization

Thermodynamic and kinetic aspects of the partial oxidation of glucose (Sigma-Aldrich) and fructose (Sigma-Aldrich) were investigated via cyclic voltammetry (CV) in a 0.5 M Na_2SO_4 (99% Sigma-Aldrich), both in the absence and presence of 0.1 M of biomass. Cyclic voltammetry measurements were conducted by employing a Parstat 4000 potentiostat within the voltage range of 0 to 1.9 V vs RHE, utilizing a three-electrode cell configuration with Pt mesh serving as the working and counter electrode, and Ag/AgCl/3.5 M KCl as the reference electrode. A scan rate of 5 mV/s was employed. For the sake of comparison, CVs were plotted using the Reverse Hydrogen Electrode (RHE) potential, as described in Equation (1).

$$E_{RHE}\ (V) = 0.198 + 0.059\,pH + \ E_{Ag/AgCl} \qquad (1$$

where $E_{Ag/AgCl}$ is the working potential.
Scanning electron microscopy (SEM) images were captured using a FEI Quanta 200 ESEM microscope operating at 30 kV. X-ray diffraction (XRD) patterns of the photoanodes were obtained at room temperature utilizing a PANalytical Empyrean diffractometer equipped with a PIXcel1D detector operating at 40 kV and 40 mA, utilizing CuKa radiation, and with a 2θ scan rate of 3°/min.
Raman spectra were acquired using a Raman Microscope coupled with a Leica DMLM microscope. The laser was focused onto the sample through a 5x magnification lens to achieve an analyzing spot diameter of approximately 50 µm, with a maximum laser power of 133 mW. Only 10% of the maximum power was utilized, reduced by holographic filters (three for each sample). Spectra were recorded using a 532 nm laser coupled with a 2400 lines per millimeter grating, resulting in a spectral resolution of 0.5 cm^{-1}. Each measurement comprised two accumulations.
For the photoelectrochemical measurements, the TiO_2 nanotubes photoanode served as the working electrode in a three-electrode cell configuration, with a Pt wire as the counter electrode, and an Ag/AgCl/saturated KCl reference electrode. A 0.1 M ammonium biborate tetrahydrate (ABE, $(NH_4)_2B_4O_7 \cdot 4H_2O$; Sigma Aldrich), was employed as the electrolyte. The UV–vis Xenon lamp, with a power of 450 W, was employed. Its light was directed to a monochromator to enable selective wavelength irradiation of the sample surface through the quartz window of the cell. The electrode

potential was regulated by a versastat potentiostat. To obtain the photocurrent spectra (i.e., photocurrent vs wavelength) by applying 0.5 V vs Ag/AgCl, the resulting current was directed to a two-phase lock-in amplifier to separate the photocurrent from the total current circulating in the cell. A mechanical chopper was utilized to halt irradiation at a predetermined frequency, specifically 13 Hz. Photocurrent spectra were reported in the text as photocurrent yield (Q_{ph}). This yield was calculated by considering the relative photon flux of the light source at each wavelength, reflecting the efficiency of the lamp-monochromator system.

Mott-Schottky (M-S) analysis was conducted under dark conditions by varying the applied potential from 1 V to -0.7 V vs. Ag/AgCl with a sinusoidal modulation of the applied potential of 10 mV amplitude and a frequency of 1 kHz.

Electrochemical Impedance Spectroscopy (EIS) measurements were conducted using a Parstat 4000 potentiostat equipped with an Impedance Analyzer connected to the cell. Impedance spectra were recorded over the frequency range of 100 kHz to 0.1 Hz at 25°C, applying 1 V between the photoanode and the cathode, and employing an AC amplitude of 10 mV. Before each measurement, the cell was allowed to stabilize for at least 15 minutes under irradiation. Data analysis and equivalent circuit fitting were performed using VersaStudio and ZSimpleWin software.

2.3. Photoelectrocatalytic test

Photoelectrocatalytic experiments were conducted utilizing TiO_2 NTs as the photoanode, Ni foam as the cathode, and 0.5 M Na_2SO_4 as the electrolyte. A scheme of the experimental setup is reported in Figure 1. The pH was adjusted to 2 or 12 using H_2SO_4 or NaOH, respectively, and a potential of 1 V was applied between the photoanode and the cathode for three hours. Glucose or fructose concentrations were 0.1 M. The reactions took place in undivided glass cells, employing a two-electrode configuration. As the light source, a medium-pressure Hg lamp emitting mainly near-UV light at a wavelength of 365 nm (125 W) was used. Photoanode and cathode surfaces were 90 cm^2 (irradiated) and 180 cm^2, respectively. A Parstat 4000 (PAR) potentiostat equipped with Electrochemical Impedance Spectroscopy (EIS) capabilities was utilized to regulate cell potential and gather kinetic data for both anodic and cathodic processes.

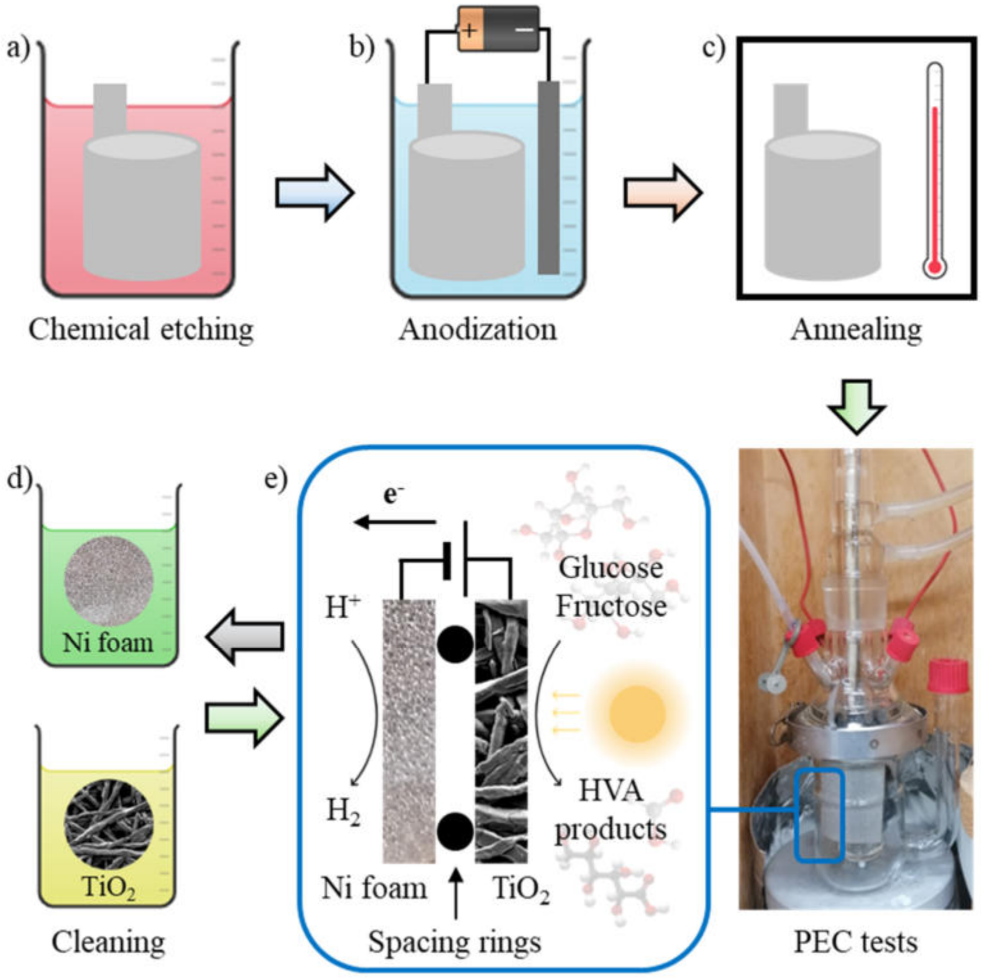

Figure 1. Scheme of the employed experimental setup. a) – c) photoanodes preparation, d) electrodes' cleaning, and e) images of the PEC cell and scheme with the reactions involved.

Before each run, Helium was bubbled under stirring in the dark for 30 minutes within the biomass aqueous solution to eliminate oxygen from the system and saturate the electrode surfaces with the substrate. Subsequently, the reactor was sealed, and the lamp was turned on. During the reaction time, water was circulated in the reactor cooling jacket to maintain the room temperature within the reaction mixture.

The photoanode was subjected to reuse after sonication with acetone and water for 5 minutes each to eliminate any glycerol residues, while Ni foam was cleaned by sonication for 5 minutes in 1 M HCl and water.

2.4. Analitycal tecniques

The detection and quantification of glucose, fructose, and reaction intermediates were conducted using a Thermo Scientific Dionex UltiMate 3000 HPLC, equipped with a Diode Array detector and a REZEK ROA Organic acid H^+ column. Analysis of gaseous species collected in the reactor headspace was carried out using an HP 6890 Series GC system, featuring a Supelco GC 60/80 CarboxenTM-1000 packed column and a thermal conductivity detector.

The faradic efficiency for GA, FA, CO_2, and H_2 was determined using Equation (2):

$$FE\ (\%) = \frac{Amount\ of\ product\ i\ formed\ (mol)}{\frac{Q\ (Coulomb)}{z\ F\ \left(\frac{Coulomb}{mol}\right)}} \quad (2$$

where:

- i is the formed product
- Q is the circulated charge
- z are the electrons exchanged, that are equivalent to the number of holes reported in Table 2 considering the half-reactions in Equations. (3) - (6)
- F is the Faraday constant of 96,485 [Coulomb/mol]

$$C_6H_{12}O_6 + H_2O + 2\,h^+ \rightarrow C_6H_{12}O_7 + 2\,H^+ \quad (3$$

$$C_6H_{12}O_6 + 6\,H_2O + 12\,h^+ \rightarrow 6\,CH_2O_2 + 12\,H^+ \quad (4$$

$$C_6H_{12}O_6 + 6\,H_2O + 24\,h^+ \rightarrow 6\,CO_2 + 24\,H^+ \quad (5$$

$$2\,H^+ + 2\,e^- \rightarrow H_2 \quad (6$$

Table 2. Electrons/holes exchanged in the half cell reactions reported in the Equations 3-6 per mol of product

Compound	Chemical formula	Electrons/holes exchanged
Glucose/fructose	$C_6H_{12}O_6$	
GA	$C_6H_{12}O_7$	2
FA	CH_2O_2	2
Carbon dioxide	CO_2	4
Hydrogen	H_2	2

3. Results and discussion

Figure 2 compares the morphological features of TiO_2 NTs grown in ammonium fluoride containing ethylene glycol solution with 50% (Figures 2a-c) and 0.75% of water (Figures 2d-f), respectively, after thermal treatment at 450 °C for 3 h. The SEM micrographs distinctly reveal the achievement of a large array of TiO_2 NTs, wherein the average length is ~ 850 nm and 720 nm respectively (inset of Figures 2a and d). Notably, NTs grown in 50%w show thinner sharp walls with a large space among NTs, thus allowing a better contact and refreshment of the electrolyte during the photoeletrochemical process. These findings are consistent with earlier investigations [41].

XRD pattern for annealed TiO_2 NTs, reported in Figures 2 b and d, shows the reflections of anatase polymorph due to the crystallization of TiO_2 grown by the anodizing process, together with the reflections of titanium arising from the not anodized metal still present beneath the nanotube layers that allows an efficient electrical contact with the photoactive titania [42]. The presence of anatase is also confirmed by Raman spectroscopy. As shown in Figure 2c and e characteristic bands of anatase polymorph are present at 144 cm^{-1}, 196 cm^{-1}, 397 cm^{-1}, 513 cm^{-1}, and 639 cm^{-1} [43].

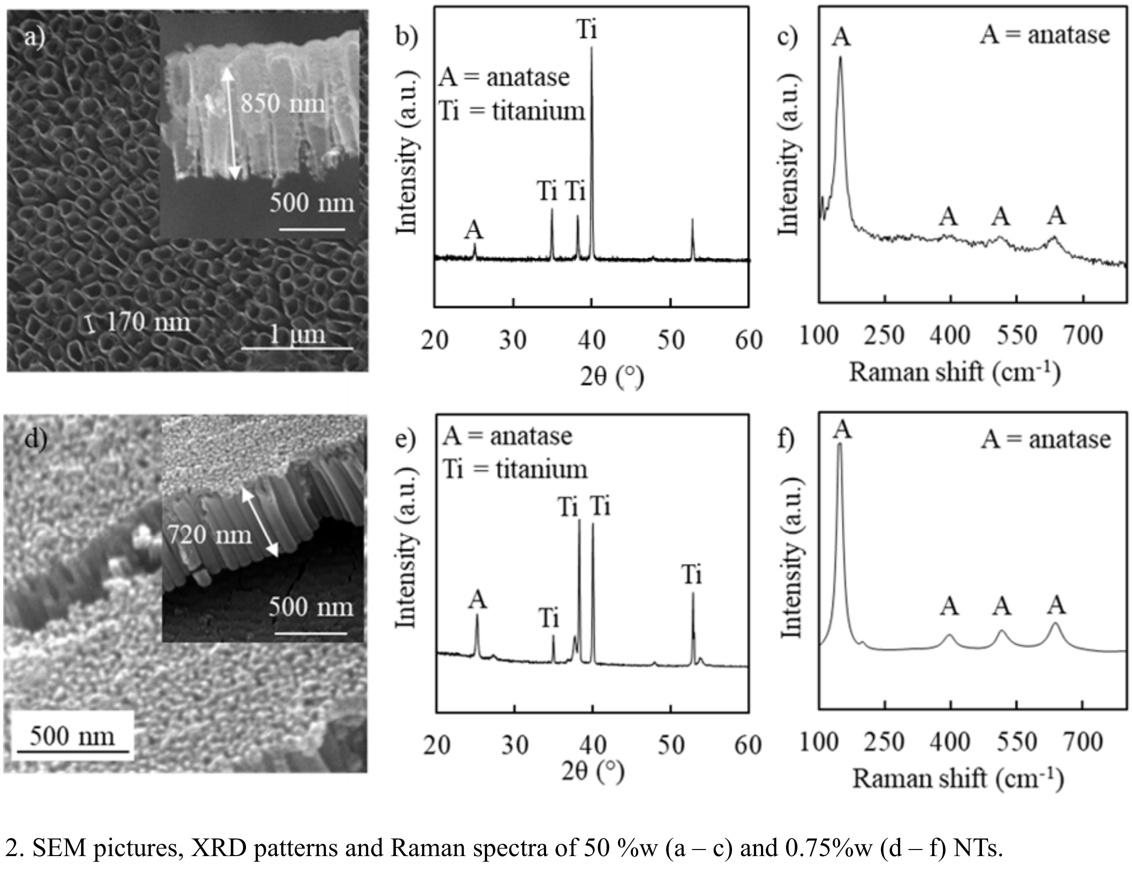

Figure 2. SEM pictures, XRD patterns and Raman spectra of 50 %w (a – c) and 0.75%w (d – f) NTs.

A photoelectrochemical investigation aimed to gain information about the electronic characteristics of the photoanodes was carried out. The photocurrent spectrum, i.e. photocurrent as a function of the monochromatic irradiating wavelength, recorded under a constant bias polarizing the Ti/TiO_2 NTs layer electrode in a 0.1 M ABE aqueous solution at 0.5 V vs Ag/AgCl, is shown in Figure 3a. Under the hypothesis of non-direct optical transitions, an estimation of the optical band gap value (Eg) was made by extrapolating to zero the $(Q_{ph} \cdot h\nu)^{0.5}$ vs hν plot (Figure 3b). The determined Eg is 3.15 eV, which is in line with the reported value for anatase (3.2 eV [41]). The photocurrent transients were measured by manually interrupting monochromatic irradiation (at λ = 340 nm), while applying a constant potential ranging from 0.5 to -0.5 V vs Ag/AgCl (see Figure 3c). An anodic photocurrent was observed, confirming the n-type semiconductor behavior of the oxide, with the photocurrent reaching zero at approximately - 0.5 V vs Ag/AgCl. The zero photocurrent potential can be considered an estimate of the flat band potential, V_{fb}. This value agrees with that estimated by the M-S plot recorded at 1 kHz reported in Figure 3d. It is important to mention that the flat band potential of TiO_2 NTs grown in water containing solution is slightly more positive than that estimated for NTs grown on ethylene glycol solution (i.e. -0.75 V Ag/AgCl [25]). This implies that the flat band potential is shifted toward the mid gap position. Additionally, the n-type behaviour of TiO_2 NTs is also confirmed by the cathodic photopotential recorded during the irradiation of the sample, as shown in Figure 3e [44].

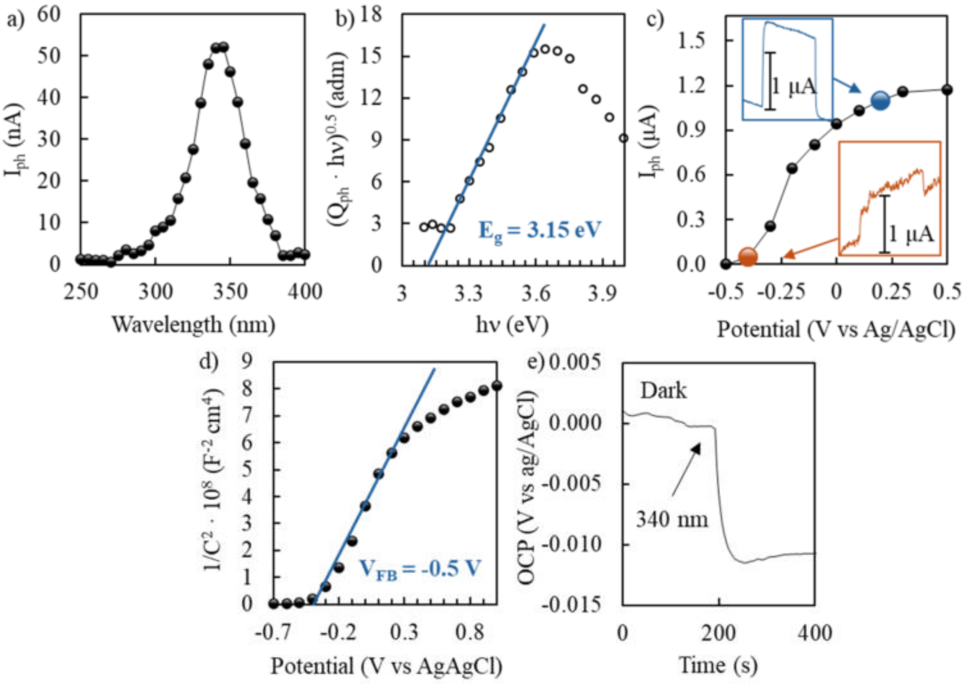

Figure 3. a) photocurrent spectra, b) E_g estimation, c) photocurrent transients, d) M-S plot, and e) photopotential recorded for 50%w NTs.

A preliminary electrochemical assessment was conducted to gather insights into the kinetics of glucose and fructose oxidation in 0.5 M Na_2SO_4 aqueous solution at different pH (i.e., 2, 7, and 12) within a potential range of 0 to 1.9 V vs. RHE. Figure 4 illustrates the cyclic voltammograms obtained in solutions without biomass and those containing either glucose or fructose, utilizing a Pt mesh as the working and the counter electrode. At pH 2 (Figure 4a), cyclic voltammogram reveals three oxidation peaks at 0.2, 0.7, and an oxidation current starting at 1.1 vs. RHE in presence of glucose or fructose, with higher values being measured with fructose. According to the literature [45] in the case of glucose the first peak corresponds to the oxidation of the adsorbed hydrogen produced by chemisorption of the glucose molecule, that however does not poison the surface of the electrode, while the second peak is assigned to the oxidation of strongly adsorbed intermediate produced from the glucose oxidation in the first process. Only at high potential (namely 1.6 V vs RHE), oxygen evolution occurs suggesting that both glucose and fructose oxidation is more favorable. Notably, the OER is not significantly affected by the presence of the biomass, i.e., the current recorded at higher potential is comparable with and without biomass in the electrolyte.

The cyclic voltammograms recorded at pH 7 (Figure 4b) show three peaks at 0.2, 0.9, and a more pronounced one at 1.4 V vs RHE only when glucose is present with the anodic current starting at 1.1 V vs RHE. According to the literature [46], the oxidation current at 0.2 V vs RHE is associated to the production of the carboxylic acids such as gluconic acid, glucuronic acid and/or glucaric acid with a higher selectivity towards the generation of gluconic acid. The reaction proceeds through a complex mechanism, in which at first step glucose is oxidized to gluconic acid, and the when the potential is increased, gluconic acid generates CO species and cyclic carbonate, and both are practically completely removed from the electrode surface when they are oxidized to CO_2. According to the cyclic voltammogram recorded in biomass free solution, OER starts at ~ 1.5 V vs RHE. No peaks are observed with fructose, although an increased faradic current indicating its oxidation is noted by comparing the cyclic voltammetry recorded without and with fructose.

At pH 12 (Figure 4c), the cyclic voltammograms show multiple peaks in presence of biomass, suggesting that several oxidation steps occur by increasing the applied potential involving oxidation of glucose or fructose. According to the literature [47,48] the first peak corresponds to the oxidation of the adsorbed hydrogen produced by glucose chemisorption, while peaks at 0.7 V vs RHE corresponds to the direct oxidation of glucose from the bulk. Finally, peak at 1.1 V vs RHE corresponds to the oxidation of the adsorbed species resulting from the chemisorption of glucose occurring at lower potential. At this pH, OER appears to be partially inhibited in presence of fructose since water oxidation starts only at 1.7 V vs RHE, while with glucose event at 1.9 V vs RHE there is no evidence of a current due to O_2 evolution.

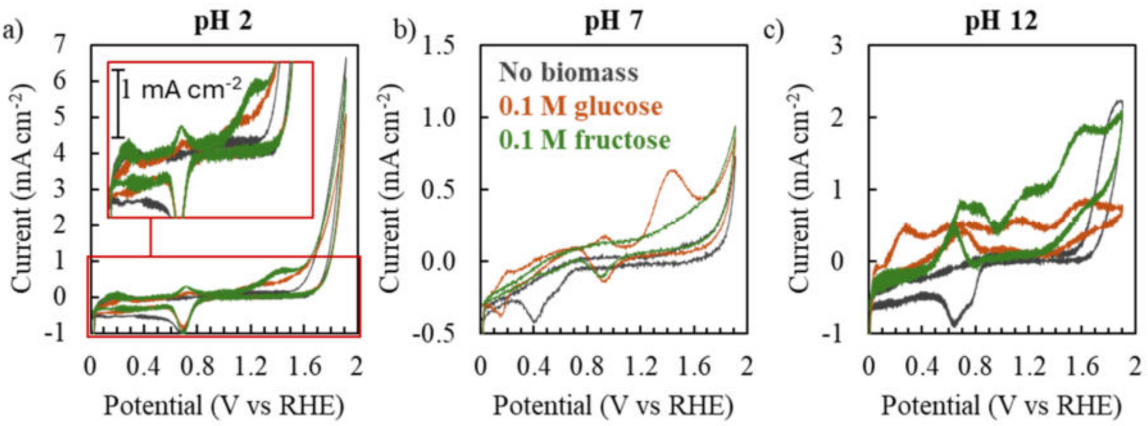

Figure 4. Cyclic voltammetries carried out at a) pH 2, b) pH 7, and c) pH 12 with and without the presence of biomass.

Figure 5 summarizes the results of the photoelectrochemical electrolysis of glucose and fructose containing solutions at different pH (namely pH 2, 7 and 12), carried out under a bias of 1 V using the TiO_2 NTs photoanodes. First of all, it is important to stress that the measured photocurrent is comparable to that measured in biomass free solution (see Figure S1a), but with higher hydrogen evolution rate due to the Faradic efficiency of 100% or slightly lower than 100 % for glucose and fructose containing solutions, respectively, in spite the use of undivided cell. Moreover, I_{ph} is higher for NTs grown in solution with a low concentration of water, probably due to the higher thickness of the tubes' wall allowing a more efficient light absorption [39,49], but also to a more negative flat band potential with respect to NTs grown in 50%w solution. Indeed, the electric field driving the transport of photogenerated holes and electrons is directly connected to the band bending, $\Delta\Phi_{SC} = U_E - U_{FB}$. Finally, for NTs grown with a low water concentration the measured photocurrent is slightly influenced by the electrolyte pH, the lowest value being measured in neutral solution. Conversely, the measured photocurrent is almost independent on the pH for TiO_2 NTs grown with a high concentration of water.

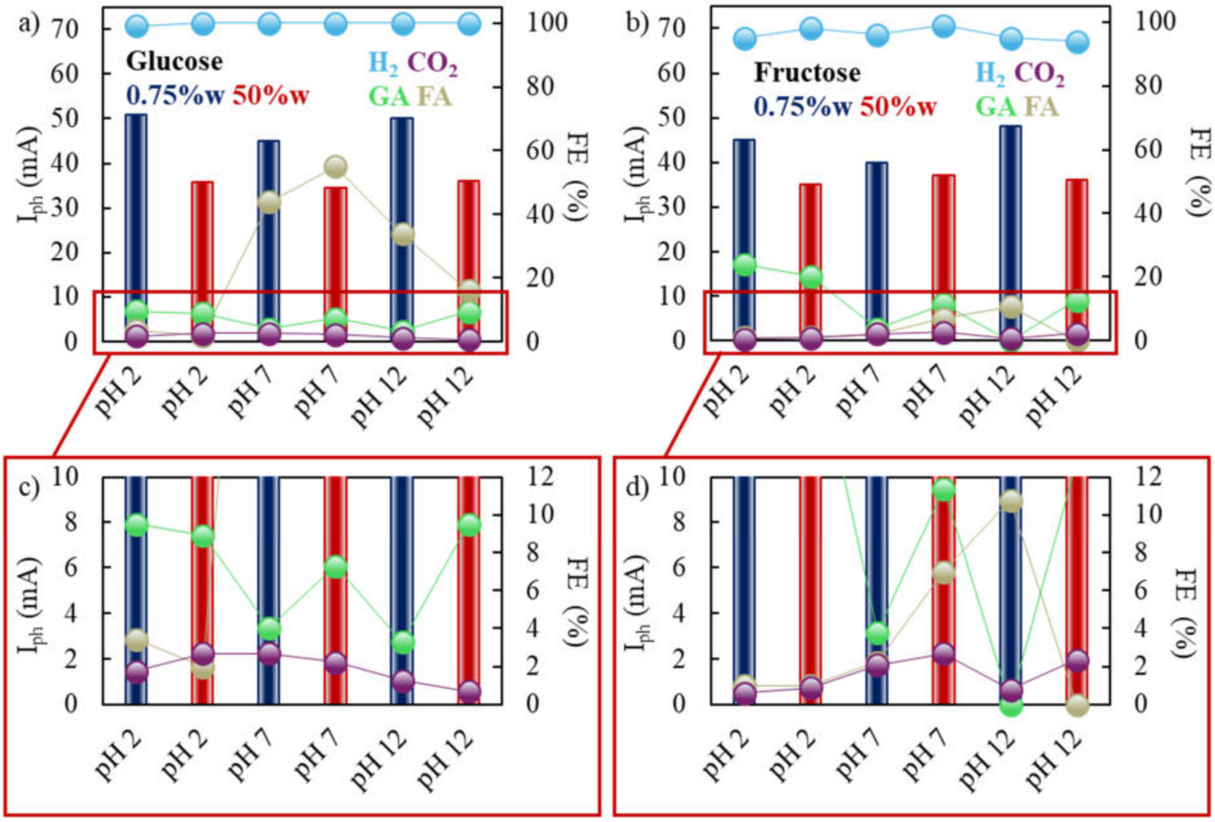

Figure 5. Photoelectrochemical results obtained by using a) c) glucose or b) d) fructose as the starting biomass.

A clear idea of the products of the photoelectrochemical reactions is provided by the plots of Figure 5, showing the faradic efficiencies for both the employed photoanodes as a function of the pH. For glucose, in slightly acidic solution the most abundant product is GA (FE ~ 8%) followed by FA and CO_2. This finding can be explained by CV recorded in the same solution showing very low current due to glucose oxidation and an onset potential for oxygen evolution close to the third oxidation step involving glucose.

Better results were obtained in neutral solution, where partial oxidation of glucose leads to a very high faradic efficiency in FA, even if FE for GA is lower than that measured at pH 2. At this pH according to the CV of Figure 4b, the third glucose oxidation step occurs at potential significantly lower than that of O_2 evolution, which is therefore significantly less favourable on a kinetic point of view. At pH 12 the most favourable reaction is partial oxidation of glucose to FA, but with lower FE than that estimated at pH 7. These results were compared with those reported in the literature [26] by normalizing the HVA and H_2 production rates by considering the photoanode area and incident photon flux. As shown in Table 3, our work achieved better performances in both cases, despite the larger photoanode area and the use of PGM-free materials.

Table 3. Comparison with the literature of HVA and H_2 production rates normalized by photoanode area and incident photon flux.

	[26]	This work
Photoanode	Pt(SA)/def-TiO_2 NRs[(a)]	TiO_2 NTs
Cathode	Pt foil	Ni foam
Biomass	Glucose 0.01 M	Glucose 0.1 M
Electrolyte	1 M KOH	0.5 M Na_2SO_4 pH 7
Applied bias	0.6 V vs RHE	1 V
Photoanode area (cm^2)	1	90
Light source (mW cm^{-2})	100	10
HVA production rate (μmol h^{-1} mW^{-1})	0.340[(b)]	0.565[(c)]
H_2 production rate (μmol h^{-1} mW^{-1})	0.356	0.933

(a) Defective TiO_2 nanorods decorated with Pt single atom

(b) Considering both gluconic and glucaric acid

(c) Considering both gluconic and formic acid

Different results were obtained by photoelectrolysis of fructose containing solutions. At pH 2 the photoelectrochemical oxidation of the biomass leads to the formation of GA with FE = 24% and 20.3% for NTs grown in 0.75% water and 50% water, respectively. This finding agrees with the results of the cyclic voltammetry showing a better kinetic for fructose oxidation in acidic solution. Lower faradic efficiencies for both GA and FA are estimated at higher pH, making the process less promising with respect to the photoelectrolysis of glucose.

Electrochemical impedance spectra were recorded under 1 V of bias during photoelectrolysis of both glucose and fructose. Figure 6 shows the corresponding spectra in the Nyquist representation recorded under irradiation. For comparison we also recorded impedance spectra in biomass free solution (i.e. water photoelectrolysis), that are reported in Figure S1 b-c, with the relative fitting parameters in Tables S1-2. All the spectra are slightly depressed semicircles, thus they can be fitted with the very simple equivalent circuit of Figure 6, where R_{CT} is the charge transfer resistance, Q_{SC} the capacitance of the semiconductor under irradiation, while R_{el} accounts for the electrolyte resistance. The corresponding fitting parameters are summarized in Table 3. At a first glance it is evident that a constant phase element is necessary to simulate the non-ideal capacitance of TiO_2 NTs layer (see exponent $n < 1$). Using the Brug formula [50] it is possible to estimate the NTs capacitance, that results slightly higher for NTs grown in solution with a lower concentration of water. This is in agreement with a higher concentration of donors as suggested by the more negative flat band potential measured for these NTs [25]. The higher doping level and the consequent higher concentration of charge carriers under irradiation explain the higher photocurrent measured for these NTs with respect to those grown in 50%water. Table 3 also reports the charge transfer resistance for both glucose and fructose oxidation at different pH and for both NTs layers. According to Table 4, the charge transfer resistance ranges from 1.3 to 2.3 kΩ cm^2, with the lowest value being measured during photoelectrolysis of glucose containing solution at pH 7 by employing 0.75%w NTs. Notably, it is interesting to mention that the charge transfer resistance is inversely proportional to the overall Faradic efficiency in biomass oxidation products due to the sluggish kinetic of oxygen evolution reaction affecting the overvoltage necessary to activate the reaction. The charge transfer resistances estimated during the photoelectrolysis of fructose containing solution are comparable to those estimated for glucose photooxidation despite the lower photocurrent in agreement with a lower overall faradic efficiency and consequent higher photocurrent wasted for O_2.

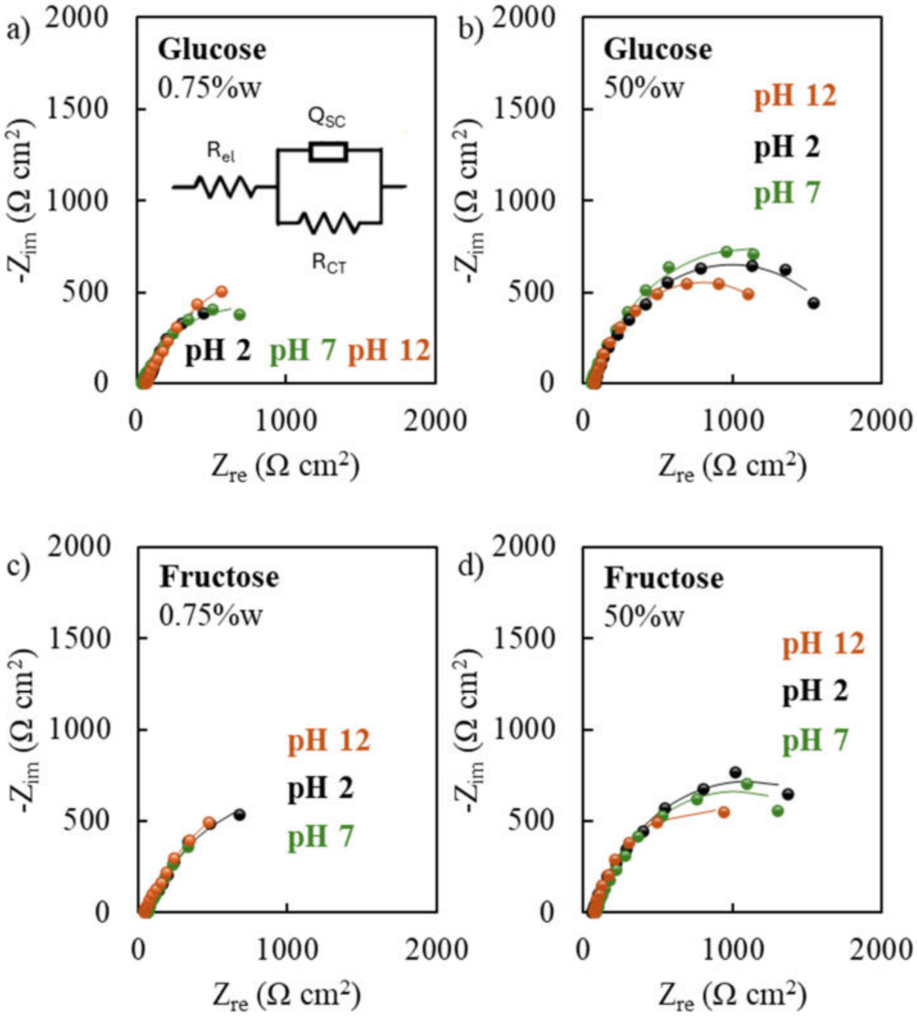

Figure 6. In situ EIS spectra recorded under irradiation in the presence of glucose a) – b) and fructose c) – fd. All the spectra were fitted by using the equivalent circuit shown in the inset of a).

Table 4. Fitting parameters obtained by EIS spectra recorded under irradiation.

Sample	**pH**	**Substrate**	**R_{el} (Ω cm^2)**	**R_{CT} (Ω cm^2)**	**Q_{SC} (μS s^n cm^{-2})**	**n (adm)**	**C_{Brug} (μF cm^{-2})**	**χ square (adm)**
0.75%w	2	Glucose	58	$2.3 \cdot 10^3$	$1.8 \cdot 10^{-3}$	0.68	622	$5.2 \cdot 10^{-3}$
50%w	2	Glucose	79	$1.8 \cdot 10^3$	$3.5 \cdot 10^{-4}$	0.79	135	$1.2 \cdot 10^{-3}$
0.75%w	2	Fructose	59	$2.0 \cdot 10^3$	$9.6 \cdot 10^{-4}$	0.71	297	$2.1 \cdot 10^{-3}$
50%w	2	Fructose	61	$2.1 \cdot 10^3$	$3.7 \cdot 10^{-4}$	0.77	119	$1.1 \cdot 10^{-3}$
0.75%w	7	Glucose	36	$1.3 \cdot 10^3$	$1.2 \cdot 10^{-3}$	0.72	354	$4.1 \cdot 10^{-3}$
50%w	7	Glucose	55	$2.1 \cdot 10^3$	$4.6 \cdot 10^{-4}$	0.78	163	$1.4 \cdot 10^{-3}$
0.75%w	7	Fructose	63	$1.7 \cdot 10^3$	$1.5 \cdot 10^{-3}$	0.73	627	$9.7 \cdot 10^{-4}$
50%w	7	Fructose	86	$1.9 \cdot 10^3$	$5.6 \cdot 10^{-4}$	0.78	238	$1.6 \cdot 10^{-3}$
0.75%w	12	Glucose	64	$1.8 \cdot 10^3$	$1.2 \cdot 10^{-3}$	0.75	510	$1.4 \cdot 10^{-3}$
50%w	12	Glucose	74	$1.5 \cdot 10^3$	$5.7 \cdot 10^{-4}$	0.82	284	$1.1 \cdot 10^{-3}$
0.75%w	12	Fructose	41	$2.4 \cdot 10^3$	$1.2 \cdot 10^{-3}$	0.69	310	$9.8 \cdot 10^{-4}$
50%w	12	Fructose	74	$1.4 \cdot 10^3$	$5.9 \cdot 10^{-4}$	0.84	325	$8.2 \cdot 10^{-4}$

4. Discussion

Figure 7 shows the energetic of Ti/TiO_2 NTs/electrolyte interface. Conduction and valence band edges were located according to the literature [25], while their flat band potential is quoted using the relationship reported in Equation (7):

$$E_F = -|e|\,V_{fb} + |e|\,V_{ref} \qquad (7$$

where V_{ref} represents the potential of the reference electrode used in the photoelectrochemical measurements.

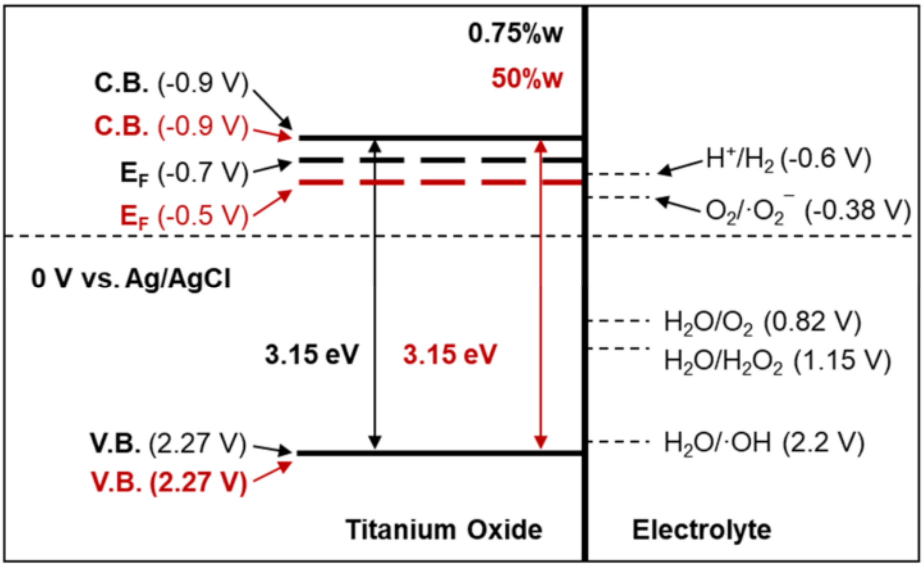

Figure 7. Sketch of the energetic levels of the metal/oxide/electrolyte interface

According to this sketch, the photogenerated holes can oxidize water to produce not only oxygen and hydrogen peroxide, but also hydroxyl radicals. This information can be used to explain the reactions going on during biomass photoelectrolysis.

The results of glucose and fructose photoelectrolysis show that a proper selection of the process conditions allows to get high value added products with simultaneous hydrogen production. Carrying out the process at pH 7 in 0.1 M glucose aqueous solution allows to convert the biomass in formic acid with a good Faradic efficiency (44% and 55% for 0.75%w and 50%w NTs respectively) with part of the anodic current being also employed to produce gluconic acid. Hydrogen is produced at the cathode with a FE of 100% Conversely, the best results starting with fructose containing solution are obtained at pH 2, where the reaction has a high selectivity toward gluconic acid whose production occurs with a Faradic efficiency of 24% and 20.3% for 0.75%w and 50%w NTs respectively.

These results suggest that glucose and fructose photoelectrochemical oxidation follows a different path. PEC oxidation of glucose to GA and FA on TiO_2 NTs photoanode starts with the generation of holes due to light absorption. The holes can oxidize water to form adsorbed •OH radicals, which in turn can oxidize the biomass (Figure 7). According to previous results reported in the literature [4,13,26,51–55], a first adsorption step is necessary for biomass oxidation and, thus, the oxidation reaction rate as well as the products depend on how strong the biomass adsorption is (Figure 8). The adsorption of glucose on TiO_2 surface is affected by the electrolyte pH, since the excess surface charge on TiO_2 depends on the pH of the solution with respect to the pH of zero charge, that for anodic TiO_2 is around 5.8 [56]. Surface hydroxyl groups are present on TiO_2 in aqueous solution, and they are involved in superficial ionization equilibria that can be described according to the Equations (8-9):

$$-TiOH_2^+ \leftrightarrow -TiOH + H^+ \quad (8$$

$$-TiOH \leftrightarrow -TiO^- + H^+ \quad (9$$

where -TiOH represent an hydroxyl group on titanium oxide surface (i.e. titanol surface group). Thus, taking into account the pH of zero charge for titania, we expect that the surface species are $-TiOH_2^+$ in acidic solution, -TiOH in neutral solution and $-TiO^-$ in alkaline conditions.

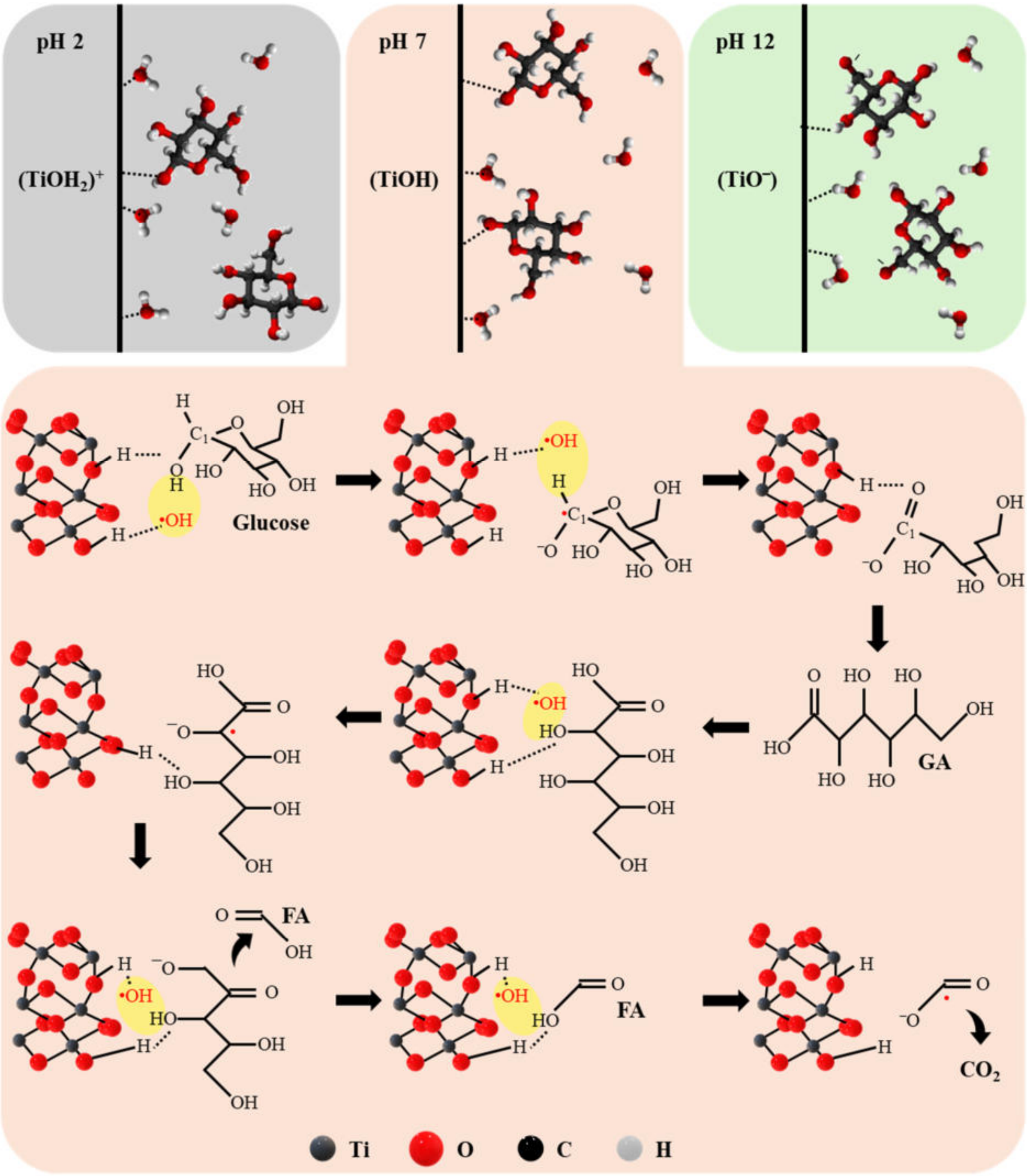

Figure 8. Schematic illustration of interaction between NTs surface, water and glucose at various pH and reaction mechanism at pH 7

Glucose molecule (RHCOH) can be adsorbed on the catalyst through hydrogen bond (indicated as ⋯). The adsorption reaction can be expressed by Equation 10:

$$-TiOH + RHCOH \leftrightarrow -TiOH \cdots OHCHR \quad (10$$

Because of the cyclic oxygen of glucose (Figure 8) can strongly affect the hydroxyl group at C_1 due to the shortest distance, the strength of hydrogen bond between -TiOH and the hydroxyl group at C_1 is much larger than those between -TiOH and other hydroxyl groups. Thus, we could assume that a glucose molecule can be adsorbed mainly at TiO_2 surface by the hydroxyl group at C_1. As soon as irradiation generates electron-hole pairs, electrons are transported by the electric field (due to the band bending) toward the cathode through the external circuit where they allow Hydrogen Evolution Reaction (HER). The holes in the valence band can oxidize water to produce hydroxyl radicals on the TiO_2 surface, i.e. TiOH+·. Adsorbed glucose (electron donor) is oxidized by these species at C_1, as shown In Equation (11):

$$-TiOH\bullet + RHCOH \leftrightarrow -TiOH_2^+ + RC\bullet OH \qquad (10$$

The formed RC•OH can react further with water and the hydroxyl radicals to produce GA. Subsequently, the C_5-O bond is split by hydrolysis, and then the GA is formed through desorption from the photoanode in agreement with previous findings reported in the literature [26]. Gluconic acid would react further with hydroxyl radicals so that C_5 compounds with formic acid are formed. Since there is no evidence of C_5 compounds among the products, these compounds are presumably converted to C_4 compounds by the further attack of radicals, followed by the formation of C_3 compounds, and so on. Finally, carbon dioxide may be the mineralization product for the photoelectrocatalytic degradation of glucose explaining the presence of only GA, FA and CO_2.

Notably, the fraction of titania where glucose is adsorbed depends on the pH due to effect on the excess charge on titania surface as well as on the possibility to find it in ionic form glucose. Indeed, pKa of glucose is about 12.3 [55]. When the pH <pKa, glucose in the solution is mainly in molecular form, while in alkaline condition, it can dissociate into RHCO−, which can be adsorbed on TiO_2 through hydrogen bonds. Due to the negative charge of the dissociated form, RHCO− captures holes more efficiently than the molecular form . However, with increasing pH the surface of titania is negatively charged, hence electrostatic repulsion between TiO− and RHCO− increases slowing down the formation rate of glucose oxidation products. This explains why the highest faradic efficiency of glucose oxidation is measured at pH 7, i.e. in a neutral solution not so far from the pH of zero charge. A different behaviour is observed with fructose that shows the highest faradic efficiency in products other than oxygen at pH 2. It is likely that the adsorption of fructose on TiO_2 surface is weaker than that of glucose in agreement with DFT calculation of the adsorption energy for both sugars [54] with a negative impact on the kinetic of fructose oxidation.

5. Conclusions

Photoelectrochemical H_2 and HVA production in PGM-free cells via glucose and fructose photo-oxidation at various pH was investigated using TiO_2 nanotubes on Ti felt with different features as the photoanode and Ni foam as the cathode, with working areas of 90 cm^2 and 180 cm^2, respectively. Photoelectrocatalytic tests in biomass containing solutions showed that their presence enhanced the H_2 production rate up to 0.933 $\mu mol\ h^{-1}\ mW^{-1}$ and ~ 100% of faradic efficiency (FE), with the formation of valuable oxidation products such as gluonic acid and formic acid up to 0.565 $\mu mol\ h^{-1}\ mW^{-1}$ and FE of 25% and 55% respectively.

Notably, this study demonstrated that the PEC oxidation of glucose and fructose using TiO_2 NT photoanodes is a promising approach for producing hydrogen and high-value-added chemicals under mild conditions. The findings highlight the importance of optimizing NTs synthesis conditions and reaction medium pH to enhance PEC performance and product selectivity. Moreover, both the photoanode and cathode demonstrated high mechanical and chemical stability, allowing reusability under the reaction conditions.

Acknowledgements

C.M.P. acknowledges support from the University of Palermo.

Author contributions: CRediT

Claudio Maria Pecoraro: Investigation, Visualization, Writing - original draft. Francesco Di Franco: Visualization. Writing - review & editing. Vittorio Loddo: Writing - review & editing. Marianna Bellardita: Writing - review & editing, Conceptualization; Supervision. Monica Santamaria: Funding acquisition, Writing - review & editing, Conceptualization; Supervision.

Reference

[1] L. Zhang, C. Jia, F. Bai, W. Wang, S. An, K. Zhao, Z. Li, J. Li, H. Sun, A comprehensive review of the promising clean energy carrier: Hydrogen production, transportation, storage, and utilization (HPTSU) technologies, Fuel 355 (2024) 129455. https://doi.org/10.1016/J.FUEL.2023.129455.

[2] S.E. Hosseini, M.A. Wahid, Hydrogen from solar energy, a clean energy carrier from a sustainable source of energy, Int J Energy Res 44 (2020) 4110–4131. https://doi.org/10.1002/ER.4930.

[3] C.M. Pecoraro, M. Bellardita, V. Loddo, D. Virtù, F. Di Franco, M. Santamaria, Photocatalytic and photoelectrocatalytic H2 evolution combined with valuable furfural production, Appl Catal A Gen 650 (2023) 118987. https://doi.org/10.1016/j.apcata.2022.118987.

[4] M. Bellardita, E.I. García-López, G. Marcì, L. Palmisano, Photocatalytic formation of H2 and value-added chemicals in aqueous glucose (Pt)-TiO2 suspension, Int J Hydrogen Energy 41 (2016) 5934–5947. https://doi.org/10.1016/J.IJHYDENE.2016.02.103.

[5] I.K.M. Yu, K.L. Ong, D.C.W. Tsang, M.A. Haque, T.H. Kwan, S.S. Chen, K. Uisan, S. Kulkarni, C.S.K. Lin, Chemical transformation of food and beverage waste-derived fructose to hydroxymethylfurfural as a value-added product, Catal Today 314 (2018) 70–77. https://doi.org/10.1016/J.CATTOD.2018.01.011.

[6] J. Lee, S. Jung, Y.T. Kim, H.J. Kim, K.H. Kim, Catalytic and electrocatalytic conversion of glucose into value-added chemicals, Renewable and Sustainable Energy Reviews 181 (2023) 113337. https://doi.org/10.1016/J.RSER.2023.113337.

[7] D. Aboagye, R. Djellabi, F. Medina, S. Contreras, Radical-Mediated Photocatalysis for Lignocellulosic Biomass Conversion into Value-Added Chemicals and Hydrogen: Facts, Opportunities and Challenges, Angewandte Chemie 135 (2023) e202301909. https://doi.org/10.1002/ANGE.202301909.

[8] W. Deng, Q. Zhang, Y. Wang, Catalytic transformations of cellulose and cellulose-derived carbohydrates into organic acids, Catal Today 234 (2014) 31–41. https://doi.org/10.1016/j.cattod.2013.12.041.

[9] K.R. Hwang, W. Jeon, S.Y. Lee, M.S. Kim, Y.K. Park, Sustainable bioplastics: Recent progress in the production of bio-building blocks for the bio-based next-generation polymer PEF, Chemical Engineering Journal 390 (2020) 124636. https://doi.org/10.1016/J.CEJ.2020.124636.

[10] S. Shinde, K. Tarade, G. Mitra, C. Rode, Integration of Heterogeneous Acid and Base Catalysis for Clean Synthesis of Jet-Fuel Precursor from Carbohydrates, ChemistrySelect 5 (2020) 392–400. https://doi.org/10.1002/SLCT.201903735.

[11] K. Alamgir Ahmad, M. Haider Siddiqui, K.K. Pant, K.D.P. Nigam, N.P. Shetti, T.M. Aminabhavi, E. Ahmad, A critical review on suitability and catalytic production of butyl levulinate as a blending molecule for green diesel, Chemical Engineering Journal 447 (2022) 137550. https://doi.org/10.1016/J.CEJ.2022.137550.

[12] K. Karádi, T.T. Nguyen, A.A. Ádám, K. Baán, A. Sápi, Á. Kukovecz, Z. Kónya, P. Sipos, I. Pálinkó, G. Varga, Structure–activity relationships of LDH catalysts for the glucose-to-fructose

isomerisation in ethanol, Green Chemistry 25 (2023) 5741–5755. https://doi.org/10.1039/D3GC01860A.

[13] M. Bellardita, E.I. García-López, G. Marcì, G. Nasillo, L. Palmisano, Photocatalytic Solar Light H_2 Production by Aqueous Glucose Reforming, Eur J Inorg Chem 2018 (2018) 4522–4532. https://doi.org/10.1002/ejic.201800663.

[14] S. Ramachandran, P. Fontanille, A. Pandey, C. Larroche, Gluconic acid: Properties, applications and microbial production, Food Technol Biotechnol 44 (2006) 185–195.

[15] J.V. Machado, M.L.A. da Silva, C.L.S. Silva, M.C.G. Correia, A.D. da Silva Ruy, L.A.M. Pontes, Catalysts and processes for gluconic and glucaric acids production: A comprehensive review of market and chemical routes, Catal Commun 182 (2023) 106740. https://doi.org/10.1016/J.CATCOM.2023.106740.

[16] Y. Chen, Y. Yang, X. Liu, X. Shi, C. Wang, H. Zhong, F. Jin, Sustainable production of formic acid and acetic acid from biomass, Molecular Catalysis 545 (2023) 113199. https://doi.org/10.1016/J.MCAT.2023.113199.

[17] D.O. Wasik, A. Martín-Calvo, J.J. Gutiérrez-Sevillano, D. Dubbeldam, T.J.H. Vlugt, S. Calero, Enhancement of formic acid production from carbon dioxide hydrogenation using metal-organic frameworks: Monte Carlo simulation study, Chemical Engineering Journal 467 (2023) 143432. https://doi.org/10.1016/J.CEJ.2023.143432.

[18] W. Deng, Y. Feng, J. Fu, H. Guo, Y. Guo, B. Han, Z. Jiang, L. Kong, C. Li, H. Liu, P.T.T. Nguyen, P. Ren, F. Wang, S. Wang, Y. Wang, Y. Wang, S.S. Wong, K. Yan, N. Yan, X. Yang, Y. Zhang, Z. Zhang, X. Zeng, H. Zhou, Catalytic conversion of lignocellulosic biomass into chemicals and fuels, Green Energy & Environment 8 (2023) 10–114. https://doi.org/10.1016/J.GEE.2022.07.003.

[19] H. Zhang, K. Yang, Y. Tao, Q. Yang, L. Xu, C. Liu, L. Ma, R. Xiao, Biomass directional pyrolysis based on element economy to produce high-quality fuels, chemicals, carbon materials – A review, Biotechnol Adv 69 (2023) 108262. https://doi.org/10.1016/J.BIOTECHADV.2023.108262.

[20] B. Zhang, B.K. Biswal, J. Zhang, R. Balasubramanian, Hydrothermal Treatment of Biomass Feedstocks for Sustainable Production of Chemicals, Fuels, and Materials: Progress and Perspectives, Chem Rev 123 (2023) 7193–7294. https://doi.org/10.1021/ACS.CHEMREV.2C00673/ASSET/IMAGES/MEDIUM/CR2C00673_0046.GIF.

[21] F.Y. Yu, Y.J. Zhou, H.Q. Tan, Y.G. Li, Z.H. Kang, Versatile Photoelectrocatalysis Strategy Raising Up the Green Production of Hydrogen Peroxide, Adv Energy Mater 13 (2023) 2300119. https://doi.org/10.1002/AENM.202300119.

[22] P. Li, Y. Liu, M.A. Mushtaq, D. Yan, Recent progress in ammonia synthesis based on photoelectrocatalysis, Inorg Chem Front 10 (2023) 4650–4667. https://doi.org/10.1039/D3QI00683B.

[23] X. Feng, X. Feng, F. Zhang, Enhanced photoelectrochemical oxidation of glycerol to dihydroxyacetone coupled with hydrogen generation via accelerative middle hydroxyl dehydrogenation over a Bi0/Bi3+ interface of a cascade heterostructure, J Mater Chem A Mater 11 (2023) 20242–20253. https://doi.org/10.1039/D3TA04326F.

[24] J. Yu, J. González-Cobos, F. Dappozze, P. Vernoux, A. Caravaca, C. Guillard, Basic comprehension and recent trends in photoelectrocatalytic systems, Green Chemistry 26 (2024) 1682–1708. https://doi.org/10.1039/D3GC03371F.

[25] C.M. Pecoraro, F. Di Franco, M. Bellardita, V. Loddo, M. Santamaria, Enhancing H2 production rate in PGM-free photoelectrochemical cells by glycerol photo-oxidation, Int J Hydrogen Energy 49 (2024) 322–336. https://doi.org/10.1016/j.ijhydene.2023.08.011.

[26] Z. Tian, Y. Da, M. Wang, X. Dou, X. Cui, J. Chen, R. Jiang, S. Xi, B. Cui, Y. Luo, H. Yang, Y. Long, Y. Xiao, W. Chen, Selective photoelectrochemical oxidation of glucose to glucaric acid by single atom Pt decorated defective TiO2, Nature Communications 2023 14:1 14 (2023) 1–12. https://doi.org/10.1038/s41467-023-35875-9.

[27] M. Grätzel, Photoelectrochemical cells, Nature 414 (2001) 338–344.

[28] S. Pitchaimuthu, K. Sridharan, S. Nagarajan, S. Ananthraj, P. Robertson, M.F. Kuehnel, Á. Irabien, M. Maroto-Valer, Solar Hydrogen Fuel Generation from Wastewater—Beyond Photoelectrochemical Water Splitting: A Perspective, Energies (Basel) 15 (2022). https://doi.org/10.3390/EN15197399.

[29] Y.H. Li, F. Zhang, Y. Chen, J.Y. Li, Y.J. Xu, Photoredox-catalyzed biomass intermediate conversion integrated with H2 production over Ti3C2Tx/CdS composites, Green Chemistry 22 (2020) 163–169. https://doi.org/10.1039/C9GC03332G.

[30] M.P. Kumar, R. Jagannathan, S. Ravichandran, Photoelectrochemical System for Unassisted High-Efficiency Water-Splitting Reactions Using N-Doped TiO2Nanotubes, Energy and Fuels 34 (2020) 9030–9036. https://doi.org/10.1021/ACS.ENERGYFUELS.0C00634/ASSET/IMAGES/LARGE/EF0C00634_0007.JPEG.

[31] A. Govind Rajan, J.M.P. Martirez, E.A. Carter, Why Do We Use the Materials and Operating Conditions We Use for Heterogeneous (Photo)Electrochemical Water Splitting?, ACS Catal 10 (2020). https://doi.org/10.1021/ACSCATAL.0C01862.

[32] T. Yao, X. An, H. Han, J.Q. Chen, C. Li, Photoelectrocatalytic Materials for Solar Water Splitting, Adv Energy Mater 8 (2018) 1800210. https://doi.org/10.1002/AENM.201800210.

[33] W. Chen, S. Liu, Y. Fu, H. Yan, L. Qin, C. Lai, C. Zhang, H. Ye, W. Chen, F. Qin, F. Xu, X. Huo, H. Qin, Recent advances in photoelectrocatalysis for environmental applications: Sensing, pollutants removal and microbial inactivation, Coord Chem Rev 454 (2022) 214341. https://doi.org/10.1016/J.CCR.2021.214341.

[34] E. Brillas, S. Garcia-Segura, Recent progress of applied TiO2 photoelectrocatalysis for the degradation of organic pollutants in wastewaters, J Environ Chem Eng 11 (2023) 109635. https://doi.org/10.1016/j.jece.2023.109635.

[35] P. Alulema-Pullupaxi, P.J. Espinoza-Montero, C. Sigcha-Pallo, R. Vargas, L. Fernández, J.M. Peralta-Hernández, J.L. Paz, Fundamentals and applications of photoelectrocatalysis as an efficient process to remove pollutants from water: A review, Chemosphere 281 (2021) 130821. https://doi.org/10.1016/J.CHEMOSPHERE.2021.130821.

[36] M. Bellardita, S. Yurdakal, B.S. Tek, Ç. Değirmenci, G. Palmisano, V. Loddo, L. Palmisano, J. Soria, J. Sanz, V. Augugliaro, Tuning the selectivity to aldehyde via pH regulation in the photocatalytic oxidation of 4-methoxybenzyl alcohol and vanillyl alcohol by TiO2 catalysts, J Environ Chem Eng 9 (2021) 105308. https://doi.org/10.1016/j.jece.2021.105308.

[37] A. Di Paola, M. Bellardita, L. Palmisano, Z. Barbieriková, V. Brezová, Influence of crystallinity and OH surface density on the photocatalytic activity of TiO2 powders, J Photochem Photobiol A Chem Complete (2014) 59–67. https://doi.org/10.1016/J.JPHOTOCHEM.2013.09.008.

[38] Y. Wang, M. Zu, X. Zhou, H. Lin, F. Peng, S. Zhang, Designing efficient TiO2-based photoelectrocatalysis systems for chemical engineering and sensing, Chemical Engineering Journal 381 (2020) 122605. https://doi.org/10.1016/J.CEJ.2019.122605.

[39] P. Roy, S. Berger, P. Schmuki, TiO2 Nanotubes: Synthesis and Applications, Angewandte Chemie International Edition 50 (2011) 2904–2939. https://doi.org/10.1002/anie.201001374.

[40] D. Kowalski, D. Kim, P. Schmuki, TiO2 nanotubes, nanochannels and mesosponge: Self-organized formation and applications, Nano Today 8 (2013) 235–264. https://doi.org/10.1016/j.nantod.2013.04.010.

[41] M. Santamaria, G. Conigliaro, F. Di Franco, F. Di Quarto, Photoelectrochemical Evidence of Cu2O/TiO2Nanotubes Hetero-Junctions formation and their Physicochemical

Characterization, Electrochim Acta 144 (2014) 315–323. https://doi.org/10.1016/j.electacta.2014.07.154.

[42] D. Reyes-Coronado, G. Rodríguez-Gattorno, M.E. Espinosa-Pesqueira, C. Cab, R. de Coss, G. Oskam, Phase-pure TiO $_2$ nanoparticles: anatase, brookite and rutile, Nanotechnology 19 (2008) 145605. https://doi.org/10.1088/0957-4484/19/14/145605.

[43] U. Balachandran, N.G. Eror, Raman spectra of titanium dioxide, J Solid State Chem 42 (1982) 276–282. https://doi.org/10.1016/0022-4596(82)90006-8.

[44] C.M. Pecoraro, M. Bellardita, V. Loddo, F. Di Franco, L. Palmisano, M. Santamaria, A facile way to synthesize noble metal free TiO2 based catalysts for glycerol photoreforming, Journal of Industrial and Engineering Chemistry 118 (2023) 247–258. https://doi.org/10.1016/j.jiec.2022.11.010.

[45] I.T. Bae, X. Xing, C.C. Liu, E. Yeager, In situ Fourier transform infrared reflection absorption spectroscopic studies of glucose oxidation on platinum in acid *, Elsevier Sequoia S.A, 1990.

[46] G.A.B. Mello, W. Cheuquepán, V. Briega-Martos, J.M. Feliu, Glucose electro-oxidation on Pt(100) in phosphate buffer solution (pH 7): A mechanistic study, Electrochim Acta 354 (2020). https://doi.org/10.1016/j.electacta.2020.136765.

[47] G. Moggia, T. Kenis, N. Daems, T. Breugelmans, Electrochemical Oxidation of <scp>d</scp> -Glucose in Alkaline Medium: Impact of Oxidation Potential and Chemical Side Reactions on the Selectivity to <scp>d</scp> -Gluconic and <scp>d</scp> -Glucaric Acid, ChemElectroChem 7 (2020) 86–95. https://doi.org/10.1002/celc.201901592.

[48] T. Faverge, B. Gilles, A. Bonnefont, F. Maillard, C. Coutanceau, M. Chatenet, In Situ Investigation of d-Glucose Oxidation into Value-Added Products on Au, Pt, and Pd under Alkaline Conditions: A Comparative Study, ACS Catal 13 (2023) 2657–2669. https://doi.org/10.1021/acscatal.2c05871.

[49] K. Lee, A. Mazare, P. Schmuki, One-dimensional titanium dioxide nanomaterials: Nanotubes, Chem Rev 114 (2014) 9385–9454. https://doi.org/10.1021/CR500061M/ASSET/IMAGES/MEDIUM/CR-2014-00061M_0039.GIF.

[50] B. Hirschorn, M.E. Orazem, B. Tribollet, V. Vivier, I. Frateur, M. Musiani, Determination of effective capacitance and film thickness from constant-phase-element parameters, Electrochim Acta 55 (2010) 6218–6227. https://doi.org/10.1016/j.electacta.2009.10.065.

[51] L. Lan, H. Daly, R. Sung, F. Tuna, N. Skillen, P.K.J. Robertson, C. Hardacre, X. Fan, Mechanistic Study of Glucose Photoreforming over TiO2-Based Catalysts for H2 Production, ACS Catal 13 (2023) 8574–8587. https://doi.org/10.1021/acscatal.3c00858.

[52] C. Shi, M. Eqi, J. Shi, Z. Huang, H. Qi, Constructing 3D hierarchical TiO2 microspheres with enhanced mass diffusion for efficient glucose photoreforming under modulated reaction conditions, J Colloid Interface Sci 650 (2023) 1736–1748. https://doi.org/10.1016/j.jcis.2023.07.081.

[53] Y. Zhu, R. Tan, C. Yang, B. Zhang, K. Deng, D. Tang, D. Ding, Efficient visible light photocatalytic performance of bismuth trioxide/titanium dioxide composite for selective conversion of glucose to arabinose and formic acid, Molecular Catalysis 554 (2024). https://doi.org/10.1016/j.mcat.2024.113818.

[54] Y. Ding, Y. Cao, D. Chen, J. Li, H. Wu, Y. Meng, J. Huang, J. Yuan, Y. Su, J. Wang, H. Li, Relay photo/thermal catalysis enables efficient cascade upgrading of sugars to lactic acid: Mechanism study and life cycle assessment, Chemical Engineering Journal 452 (2023). https://doi.org/10.1016/j.cej.2022.139687.

[55] M. Zhou, Y. Li, S. Peng, G. Lu, S. Li, Effect of epimerization of d-glucose on photocatalytic hydrogen generation over Pt/TiO 2, Catal Commun 18 (2012) 21–25. https://doi.org/10.1016/j.catcom.2011.11.017.

[56] K. Bubacz, B. Tryba, A.W. Morawski, The role of adsorption in decomposition of dyes on TiO2 and N-modified TiO2 photocatalysts under UV and visible light irradiations, Mater Res Bull 47 (2012) 3697–3703. https://doi.org/10.1016/J.MATERRESBULL.2012.06.038.